Zonal Penetration Scale of Midlatitude Oceanic Jets

DAVID MARSHALL* AND JOHN MARSHALL*

Center for Meteorology and Physical Oceanography, Department of Earth, Atmospheric, and Planetary Sciences, Massachusetts Institute of Technology, Cambridge, Massachusetts

(Manuscript received 2 April 1991, in final form 19 November 1991)

ABSTRACT

It is shown that subtle changes in the velocity profile across the seaward extension of midlatitude jets, such as the Gulf Stream, can lead to dramatic changes in the zonal-penetration scale. In particular, if $\alpha = dq/d\psi > 0$, where q is the absolute vorticity and ψ is a streamfunction for the geostrophic flow, then the jet tends to penetrate across to the eastern boundary; conversely if $\alpha < 0$, the jet turns back on itself creating a tight recirculation on the scale of order $|\alpha|^{-1/2}$. This behavior is demonstrated in a quasigeostrophic ocean model in which a jet profile is prescribed as an inflow condition at the western margin of a half-basin, and radiation conditions along the remainder of the western boundary allow the injected fluid to escape. Jet inflows with both vertical and horizontal structure are considered in one and one-half-, two-, and three-layer models.

Finally, the implications of our study for numerical simulations of ocean gyres, which frequently show sensitivity of jet penetration to horizontal and vertical resolution and to choice of boundary conditions, are discussed. In particular, it is demonstrated that poor resolution of the horizontal jet structure may lead to a dramatic reduction in penetration.

1. Introduction

A notable feature of the circulation of the subtropical gyre is the seaward-flowing inertial jet on its northern rim. The factors that determine the zonal penetration scale of the jet are not well understood. The penetration of a jet must be strongly influenced by its hydrodynamical stability, as studied in eddy-resolving models by Holland and Schmitz (1985) and, using a parametric representation of the eddy field, Ierley and Young (1988). Here, however, attention is focused exclusively on the *inertial* control of a jet; we will show that the form of the jet's cross-stream velocity profile can exert a controlling influence on its degree of penetration.

We argue that the propensity of an inertial barotropic jet to strike seaward or turn back on itself is controlled by the parameter α, given by

$$\alpha = \frac{dq}{d\psi}, \tag{1}$$

where q is the absolute vorticity:

$$q = \nabla^2\psi + f(y), \tag{2}$$

ψ is a streamfunction for the horizontal velocity $\mathbf{v} = \mathbf{k} \times \nabla\psi$ (with $\mathbf{k}$ a vertical unit vector), and f is the Coriolis parameter, a function of meridional coordinate y.

When α is positive, we assert that an unforced jet will have a tendency to resonate with a Fofonoff-like mode (Fofonoff 1954) and hence penetrate across to the eastern boundary of the basin; the actual penetration scale would then be controlled by instability in the manner explored by Holland and Schmitz (1985). When α is negative, however, we assert that the jet will resonate with a modonlike solution (Stern 1975) and therefore recirculate tightly, its penetration scale being set directly by α. The sign of α, and hence the type of response, is controlled by the cross-stream velocity profile. If the velocity profile is cusplike, as in Fig. 1a, then $\alpha > 0$; if the profile is wavelike, as in Fig. 1b, then $\alpha < 0$.

The possible role of α in influencing the penetration scale of an inertial subgyre has been examined by Greatbatch (1988) in attempting to understand the barotropic experiments of Böning (1986) and the results from multilayer eddy-resolving general circulation models. Here we take this idea further and present numerical experiments designed specifically to demonstrate the dependence of penetration on α.

In section 2, analytical solutions in which α takes on varying signs are reviewed. These include Fofonoff's (1954) boundary-layer solution in which α is positive and the "Modon" of Stern (1975) in which α is negative. Numerical experiments are presented in section 3, in which a jet is injected into a half-basin open to the west. This facilitates complete control over the pro-

* On leave from the Space and Atmospheric Physics Group, Department of Physics, Imperial College, London, United Kingdom.

Corresponding author address: David Marshall, MIT, Department of Earth, Atmospheric, and Planetary Sciences, Center for Meteorology and Physical Oceanography, Building 54, RM 1523, Cambridge, MA 02139.

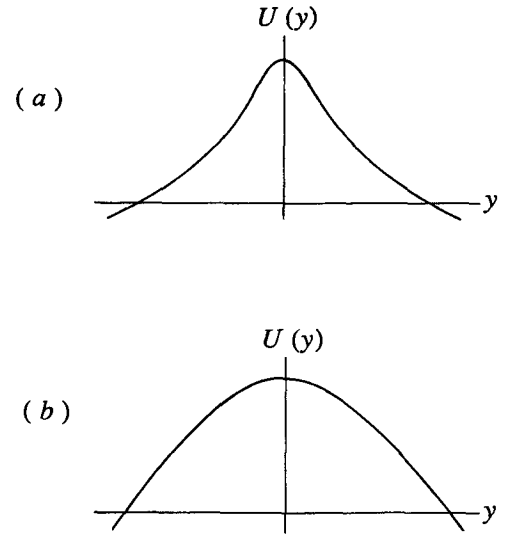

FIG. 1. Schematic diagram of the cross-stream velocity profile of (a) a penetrating jet in which $\alpha = dq/d\psi > 0$ and (b) a recirculating jet in which $\alpha = dq/d\psi < 0$, where q is the absolute vorticity and ψ is the streamfunction.

file of the inflowing jet and vividly demonstrates that α does indeed control the scale of penetration. Furthermore, it enables inflows to be investigated in which the potential vorticity is a nonlinear function of the streamfunction. Extensions to a stratified ocean are presented in section 4, in which the inflow has both vertical and horizontal structure. Finally, in section 5, implications of our results for more detailed models of the North Atlantic are discussed. In particular, we show that poor spatial resolution can lead to artificially negative values of α and hence a greatly reduced jet penetration scale.

2. Analytical background

We shall conduct our discussion in the confines of quasi-geostrophic dynamics on a β plane and adopt, initially, an equivalent barotropic model:

$$\frac{\partial Q}{\partial t} + J(\psi, Q) = 0, \tag{3a}$$

where

$$Q = \nabla^2\psi + f(y) - F\psi \tag{3b}$$

is the potential vorticity, and $F = L_\rho^{-2}$, where L_ρ is the Rossby radius of deformation. The Jacobian of a and b is $J(a, b) = \partial_x a \partial_y b - \partial_y a \partial_x b$. Here, x is an eastward-pointing coordinate, y points north, and t is time.

We have a particular interest in steady, free solutions in Eq. (3a) because they can be resonantly excited by an inflowing jet. Steady solutions to Eq. (3a) have the form

$$\nabla^2\psi + \beta y = q(\psi), \tag{4}$$

where the beta-plane approximation has been made, $f = f_0 + \beta y$, with f_0 a typical midlatitude value of the Coriolis parameter and β its gradient. Here q is the absolute vorticity.

A particular subgroup of solutions can be selected by choosing the functional relationship between q and ψ to be linear:

$$q(\psi) = \alpha\psi - c, \tag{5}$$

where α and c are assumed to be constants. Hence,

$$\nabla^2\psi + \beta y = \alpha\psi - c. \tag{6}$$

A general solution to (6) for a rectangular ocean satisfying boundary conditions of no-normal flow at walls placed at $x = \pm x_0$ and $y = 0, -y_0$ can be found in a paper by Fofonoff (1962). The form depends on the sign of α.

If $\alpha > 0$:

$$\psi = \frac{\beta y_0}{k^2}\left\{\frac{(y + y_0)}{y_0} - \frac{\sinh k(y + y_0)}{\sinh k y_0} + \frac{2}{\pi}\sum_{n=1}^{\infty}\frac{(-1)^n}{n}\left(\frac{k}{k_n}\right)^2\frac{\cosh k_n x}{\cosh k_n x_0}\sin\frac{n\pi(y + y_0)}{y_0}\right\}, \tag{7}$$

where $k_n^2 = k^2 + (n\pi/y_0)^2$, $k^2 = \alpha$, and c has been chosen to have a value $-\beta y_0$.

If $\alpha < 0$:

$$\psi = \frac{\beta y_0}{k^2}\left\{\frac{\sin k(y + y_0)}{\sin k y_0} - \frac{(y + y_0)}{y_0} - \frac{2}{\pi}\sum_{n=1}^{\infty}\frac{(-1)^n}{n}\left(\frac{k}{k_n}\right)^2\frac{\cos k_n x}{\cos k_n x_0}\sin\frac{n\pi(y + y_0)}{y_0}\right\}, \tag{8}$$

where $k_n^2 = k^2 - (n\pi/y_0)^2$, $k^2 = -\alpha$, and $c = -\beta y_0$.

For $\alpha > 0$, (Fig. 2a), the gyre fills the entire basin, while for $\alpha < 0$ (Fig. 2b), the solution consists of eddylike structures, which Fofonoff interprets in terms of time-dependent motion.

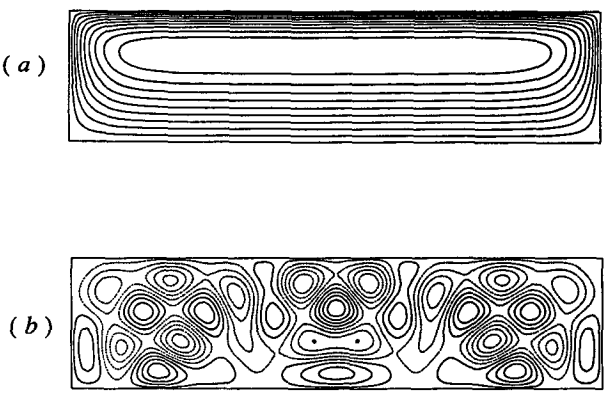

FIG. 2. An example of Fofonoff's general solution in which α is (a) positive and (b) negative.

The boundary-layer solution, presented in the seminal paper of Fofonoff (1954), is a special case of Eq. (7) appropriate when $\alpha^{-1/2} \ll x_0, y_0$,

$$\psi \approx \frac{\beta y_0}{k^2}\left\{\frac{(y+y_0)}{y_0} - e^{ky}\right\}\{1 - e^{k(x-x_0)} - e^{-k(x+x_0)}\}, \tag{9}$$

where $k^2 = \alpha$. It has a special place in canonical ocean circulation theory as reviewed by Pedlosky (1979). The gyre fills the entire basin, with inertial boundary currents of width $\alpha^{-1/2}$ on its eastern, northern, and western flanks. We show in section 3 that a jet in which α is positive can resonantly excite Fofonoff's boundary-layer mode and thus penetrate across to the eastern boundary.

But what happens if $\alpha < 0$? Fofonoff's general solution when α is negative (Fig. 2b) suggests that a jet in which $\alpha < 0$ will excite a recirculating gyre. However, if the jet recirculates tightly, then there is no reason why the $q(\psi)$ relation outside the recirculating core should be determined by the velocity profile of the jet; the $q(\psi)$ relation external to the recirculating core may take on a different value, as in the family of modon solutions. Such a flow in which α is negative inside a closed bounding streamline, and outside of which there is no flow, is given by Stern (1975):

$$\psi = \frac{\beta r_0}{k^2}\left\{\frac{J_1(kr)}{J_1(kr_0)} - \frac{r}{r_0}\right\}\sin\theta, \quad r < r_0$$

$$\psi = 0, \qquad r \geq r_0, \tag{10}$$

where $kr_0 = 5.136$, $k^2 = -\alpha$, and $r^2 = x^2 + y^2$, $\tan\theta = y/x$.

This solution, plotted in Fig. 3, consists of two regions linked by a boundary across which the streamfunction and velocity are continuous; inside the closed streamline $\alpha < 0$, outside α is in fact infinite. It exists on an infinite β plane and does not rely on the presence of boundaries. The interior recirculating region, in which α is negative, is surrounded by an exterior in which there is no flow. The recirculation is tight, and it is isolated from the rest of the basin. (To interpret Fig. 3 as a possible representation of the inertial recirculation, we consider only the positive half-plane where $x \geq 0$.) It should be contrasted to Fofonoff's boundary-layer mode in which α is positive everywhere.

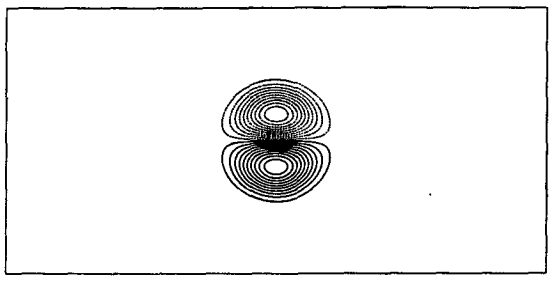

FIG. 3. A Stern modon solution on an infinite β plane. Within the closed streamline region α is negative; outside there is no flow.

Hence, we have two very distinct prototype solutions to Eq. (6), modons and Fofonoff gyres, representing two classes of free modes with which our system can resonate. Which class is excited depends on the cross-stream velocity structure of the inflowing jet. We hypothesize, and confirm by numerical experiment in section 3, that if this velocity profile is such that $\alpha > 0$, then Fofonoff-type modes will be excited and the jet will penetrate. Conversely, if $\alpha < 0$, then modon-type modes will be excited and the jet will recirculate. Furthermore, subtle changes in the cross-stream current profile can switch α from positive to negative and thereby radically alter the zonal-penetration scale.

Before describing our numerical experiments, information about penetration and recirculation scales is now deduced from the prototype solutions.

a. Zonal scale of penetration

Consider the case $\alpha < 0$. On examining Eq. (8), we see that at a particular latitude (i.e., for a constant y), the solution consists of a sum of cosines and hyperbolic cosines [since for large n in Eq. (8), k_n^2 becomes negative]. Furthermore, the term with the smallest zonal structure ($n = 1$ in the series expansion) suggests a penetration scale:

$$L_x \sim \pi|\alpha|^{-1/2}. \tag{11}$$

One might not expect such a scaling to carry over to the modon because, unlike Eq. (10), the form of the Eq. (8) derives largely from a need to satisfy boundary conditions on the walls of the basin. The modon, in contrast, is highly localized; α is uniform and negative only in the recirculating region and infinite elsewhere. Nevertheless, for a Stern modon, the condition, from Eq. (10), is

$$r_0 = 5.136|\alpha|^{-1/2}, \tag{12}$$

not unlike Eq. (11). Greatbatch (1988) has compared the prediction Eq. (12) with a variety of published numerical gyres and found some evidence of this scaling, particularly in the one-layer numerical experiments of Böning (1986).

When α is positive, it is seen from Eq. (7) that the jet always penetrates across to the eastern boundary; there is no inertial control on the zonal scale of penetration which, in the absence of flow instability, is restricted by the location of the eastern wall.

b. Meridional scale of the recirculation

Having established the possible role of α in determining the zonal penetration scale, we now examine those factors that determine the latitudinal scale of the recirculating jet. It turns out that, in addition to α, the value of the relative vorticity on the northern boundary is also of importance. If on this boundary where $y = 0$,

$\psi \equiv 0$; then in Eq. (6) the magnitude of this (negative) relative vorticity is given by c.

Consider the positive definite quantity:

$$(\nabla\psi)^2 = \nabla\cdot(\psi\nabla\psi) - \psi\nabla^2\psi \geq 0, \qquad (13)$$

which is proportional to the kinetic energy density. Integrating over the area enclosed by a closed streamline ψ_0, applying the divergence theorem, and replacing ψ by $(\psi - \psi_0)$, we obtain

$$-\int\int_A (\psi - \psi_0)\nabla^2\psi dA \geq 0. \qquad (14)$$

For an anticyclonic recirculation, the net relative vorticity within ψ_0 must be negative. But if the recirculation extends too far south, the requirement to conserve absolute vorticity along streamlines implies that the relative vorticity will, due to the variation of planetary vorticity, become increasingly positive in these southerly regions leading, eventually, to a violation of the above constraint. Hence, condition Eq. (14) *must* set a limit on the meridional extent of the recirculation.

There are two cases to be considered. When α is positive, the most negative relative vorticity is to be found on the northern rim of the recirculation. A latitudinal scale can be deduced by estimating the distance a fluid element would need to travel south in order to lose all of this relative vorticity:

$$L_y = \frac{c}{\beta}. \qquad (15)$$

Indeed, this is just the latitudinal extent of the westward return flow of a Fofonoff gyre.

The second case, in which α is negative, is more difficult to quantify. Here if $|\alpha|$ is sufficiently large, planetary vorticity gradients will be unimportant, and relative vorticity will be concentrated and most negative at the center of the recirculation where ψ is a maximum. In this limit α, rather than c, controls the latitudinal scale. Modon theory [Eq. (10)] suggests an approximate scale given by

$$L_y \sim |\alpha|^{-1/2}. \qquad (16)$$

Therefore, we suggest that when α is positive, the meridional scale is determined by c, and that as α becomes increasingly negative, the scale tends to be determined by α itself. Between these extremes, both α and c will be important.

3. Barotropic jet experiments

In order to demonstrate the resonant excitation of the solutions described in the previous section, numerical experiments are now presented in which a jet of fluid is injected from the west into a half-basin. Depending on the value of α of the inflowing jet, it either penetrates into the basin or recirculates.

a. *The model*

We use a 1½-layer version of the N-layer quasigeostrophic model described in Marshall et al. (1988). The experiments are performed in a half-basin, $2L \times L$, where L is of order 500 km, open along the western boundary.

There are three distinct boundary regions (see Fig. 4). The rigid walls of the northern, eastern, and southern boundaries are a streamline, and here ψ is set to zero. Along the western boundary, an influx and efflux of water is allowed. An inflow (i.e., a streamfunction distribution) is specified along the northern part of the boundary and held constant in time. Along the remainder of the western boundary, radiation boundary conditions are prescribed, allowing an outflow. The numerical recipe employed, due to Miller and Thorpe (1981), is described in appendix A.

In addition, along the western boundary, we assume that

$$\left(\frac{\partial^2\psi}{\partial x^2}\right)_{x=0} = 0. \qquad (17)$$

This enables $dq/d\psi$ of the inflowing jet to be specified completely in terms of the meridional velocity structure. Along the remaining solid boundaries, $\nabla^2\psi$ is extrapolated from adjacent interior grid points.

The prognostic vorticity equation (3a) is leapfrogged forward in time on the finite-difference grid. The spatial resolution of the model is $\Delta = L/48 \sim 10$ km if $L \sim 500$ km. Typically, a time step of 0.1 days was used. All the prescribed inflows have total transports consistent with observations of the North Atlantic Gulf Stream recirculation for this choice of L, that is, approximately 50 Sv (Sv $\equiv 10^6$ m^3 s^{-1}) recirculating in the subtropical gyre. In interpreting the transport of our 1½-layer model, we have assumed an effective depth of one kilometer. In the following experiments, the width of the imposed jet is approximately $L/5$ or $\sim$100 km.

The model is unforced, apart from the use of a weak biharmonic diffusion; a term of the form $\nu\nabla^6\psi$ is employed on the right-hand side of Eq. (3a) to smooth the vorticity field at the scale of the grid. Consequently, an additional higher-order boundary condition is re-

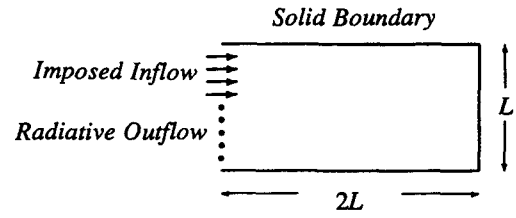

FIG. 4. Schematic diagram of the model domain. An inflow is prescribed and held fixed in time at the northern sector of the western boundary. Along the remainder of this boundary, a radiative boundary condition allows outflow. The streamfunction is set to zero along the remaining solid boundaries.

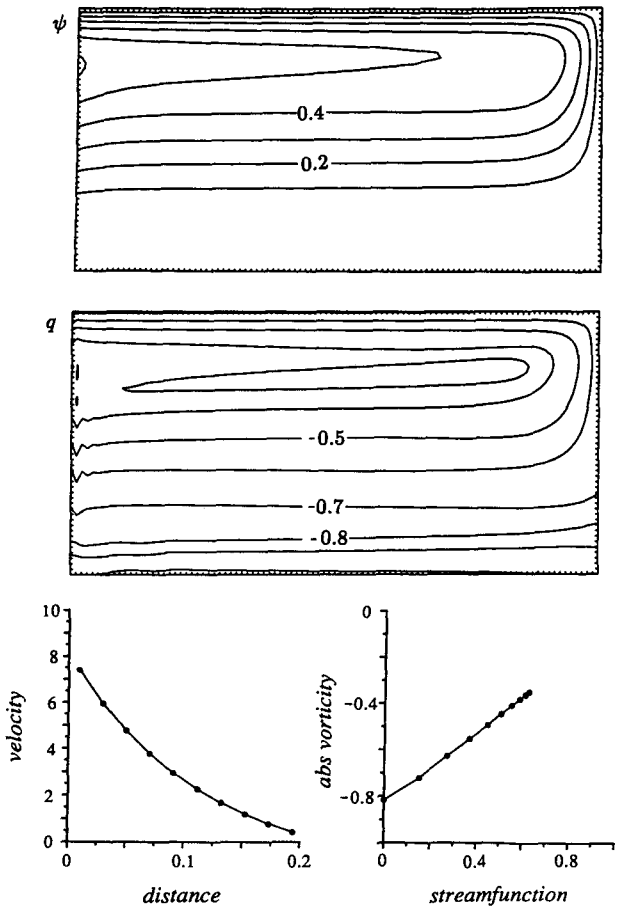

FIG. 5. The steady-state solution resulting from a Fofonoff boundary-layer inflow. The streamfunction, ψ, is presented in units of $10^{-2}\beta L^3$, and the absolute vorticity, q, in units of βL. (The same convention is employed in all subsequent figures.) The two graphs show the $q(\psi)$ relationship and jet velocity profile across the imposed inflow. Latitudinal distance is in units of L measured away from the northern wall, and the velocity is given in units of $10^{-2}\beta L^2$. If $\beta = 1.6 \times 10^{-11}$ m^{-1} s^{-1} and $L = 500$ km, then a nondimensional velocity of unity corresponds to a current speed of 4 cm s^{-1}; thus, the jet peaks at a speed of 30 cm s^{-1}.

quired and $\nabla^4\psi = 0$ is imposed. We choose a biharmonic coefficient of magnitude $\nu = \beta\Delta^5$, where Δ is the grid spacing. For a Δ of 10 km, ν has a value of $\sim 10^9$ m^4 s^{-1}, implying a vorticity spindown time scale of 100 days on the grid scale of the model if a value $\beta = 1.6 \times 10^{-11}$ m^{-1} s^{-1} is assumed. There is no bottom friction. We have tested the sensitivity of our experiments to our level of biharmonic diffusion. Our results are robust to order of magnitude variations of ν; the solutions are to first approximation free—see section 3b (7).

b. *Results*

1) FOFONOFF GYRE

A jet inflow profile was imposed with the functional form of Fofonoff's boundary-layer solution [Eq. (9)]. Note the cusplike form of the inflow velocity profile. The interior of the basin was initialized with a variety of streamfunction distributions; a Fofonoff gyre was obtained filling the entire basin in each case. Figure 5 shows the solution after 10 years of integration, and should be compared with Fig. 2a, the analytical solution.

2) NONLINEAR FOFONOFF GYRE

In an attempt to obtain a Fofonoff mode with a nonlinear functional relation between q and ψ, the following inflow was imposed:

$$\psi_{\text{inflow}} = 2\psi_{\text{Fofonoff}}, \tag{18}$$

that is, the value of the inflow streamfunction used in section 3b(1) was doubled, thus destroying the linear relation between streamfunction and potential vorticity. Nevertheless, our solution retained all general features of a conventional Fofonoff gyre, as can be seen in Fig. 6. Note the increased meridional extent of the gyre; the magnitude of the relative vorticity on the northern boundary is twice that of the previous experiment, and hence, as anticipated by Eq. (15), the meridional scale is increased. In this particular case, it is limited by the southern boundary of the basin.

3) MODONS

Initially, a jet inflow was prescribed given by Stern's modon solution; it has a wavelike inflow velocity profile. As expected, a tight recirculation is obtained, but

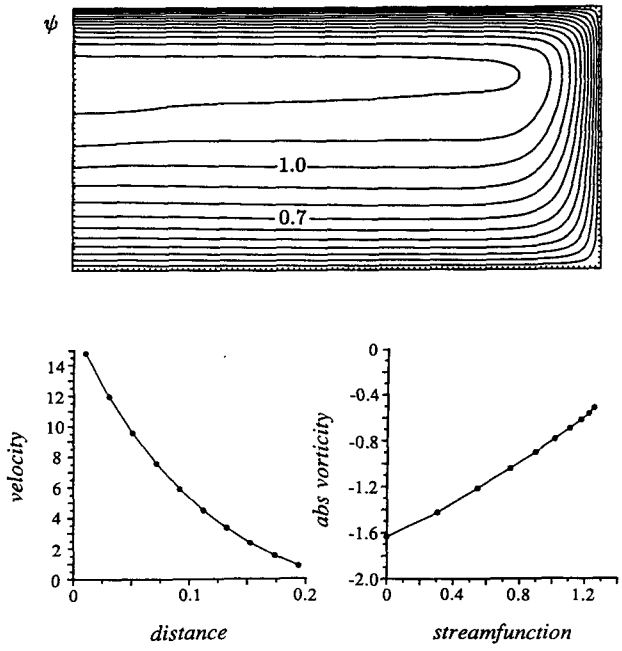

FIG. 6. The steady-state solution arising when an inflow profile of twice the strength of Fig. 5 is prescribed. Notice how the $q(\psi)$ relation is nonlinear, and yet the solution is still of Fofonoff character.

accompanied by some time-dependent motion in the exterior, which in the time-mean state averages to zero (Fig. 7). This is a consequence of both finite resolution of the model and imperfect nature of the radiation boundary conditions, most evident in the potential vorticity field of Fig. 7.

We also tried relaxing the constraint [Eq. (12)] and chose instead values in the range:

$$3.83 < |\alpha|^{1/2} r_0 < 5.136. \quad (19)$$

Such modons are only stationary in the presence of a uniform zonal flow in the far field (Larichev and Reznik 1976). Nevertheless, a tight recirculating solution is still obtained but it coexists with strong time-dependent features in the far field. However, in the time-averaged state, a pattern very similar to that of a Stern modon is obtained: a recirculating region in which α is negative, with virtually no mean flow in the exterior.

4) SINE JET

An inflow profile was prescribed of the form:

$$\psi_{\text{inflow}} = \psi_0 \sin(-ky). \quad (20)$$

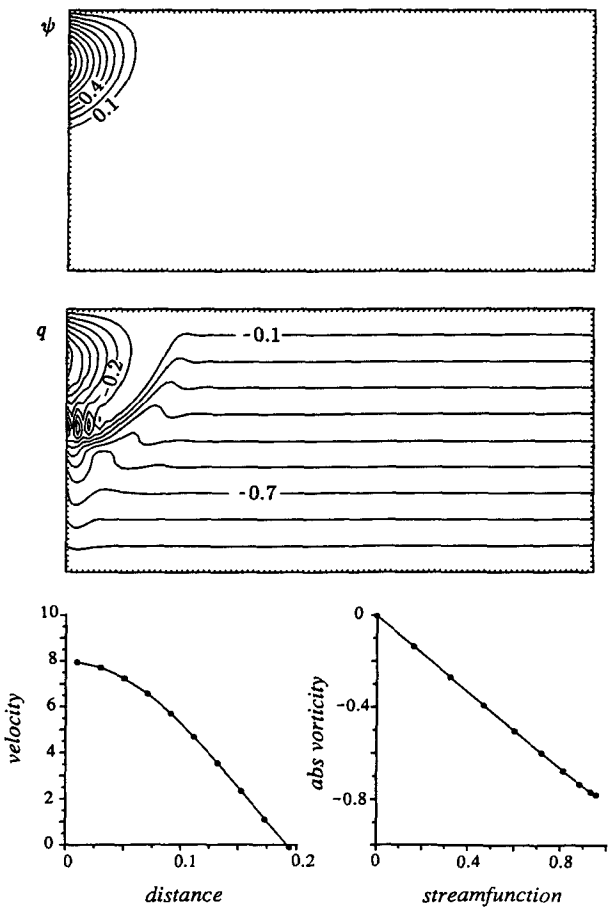

FIG. 7. The steady-state solution resulting from use of a Stern modon inflow profile. The flow is confined to a tight recirculation.

In this example, α is negative but not uniform. A tight recirculating solution, with time-dependent structures in the exterior, is obtained. The time-averaged streamfunction again resembles that of a Stern modon, see Fig. 8.

5) UNIFORM ABSOLUTE VORTICITY JETS

Setting $\alpha = 0$ in Eq. (6) gives

$$\psi_{\text{inflow}} = \frac{\beta y_0^3}{6}\left[\frac{(y + y_0)}{y_0} - \left(\frac{(y + y_0)}{y_0}\right)^3\right]. \quad (21)$$

With this inflow profile, a solution is obtained that has a strong resemblance to a Fofonoff mode; see Fig. 9. This $\alpha = 0$ case is consistent with both classes of solution; Fig. 9 can be viewed either as a Fofonoff gyre or as a modon with an infinite recirculation radius. From either perspective, the recirculation fills the entire basin zonally.

6) OBSERVING THE CHANGE OF BEHAVIOR OF THE SOLUTION

To observe the transition from a tight recirculating gyre to a penetrating jet, we experimented with a mixed modon–Fofonoff inflow given by

$$\psi_{\text{inflow}} = (1 - \chi)\psi_{\text{modon}} + \chi\psi_{\text{Fofonoff}}, \quad (22)$$

where ψ_{modon} is the modon profile used in section 3b(3), and ψ_{Fofonoff} is the Fofonoff profile of section 3b(1).

One consequence of this choice of inflow condition is that the transport changes slightly as χ is varied. However, this effect is small and not important. Values of χ between 0.2 and 0.4 are presented that change the inflow profile from a wavelike to a cusplike one. As χ increases, the jet penetrates further and further toward the eastern wall until the gyre fills the entire basin, see Fig. 10. For each inflow α is remarkably constant and clearly becomes less negative as χ increases. The penetration scale is even more sensitive to changes in α than predicted by Eq. (11). Figure 10 vividly demonstrates the role of α in controlling the penetration scale of the inflowing jet. It is remarkable that such a subtle change in velocity inflow profile can have such a dramatic effect on its penetration properties.

7) SENSITIVITY OF THE RESULTS TO THE LEVEL OF EXPLICIT DIFFUSION

In a recent study, Ierley and Young (1988) showed that jet penetration can depend on the Reynolds number of the flow, where, in this context, Re is a measure of the importance of mixing of potential vorticity by a subgrid-scale geostrophic eddy field, represented parametrically through a term $\kappa\nabla^2 q$. In particular, in the limit of very high Reynolds number (weak dissipation), their gyre, in which $\alpha = 0$, extended across to the eastern boundary as one would expect. The present

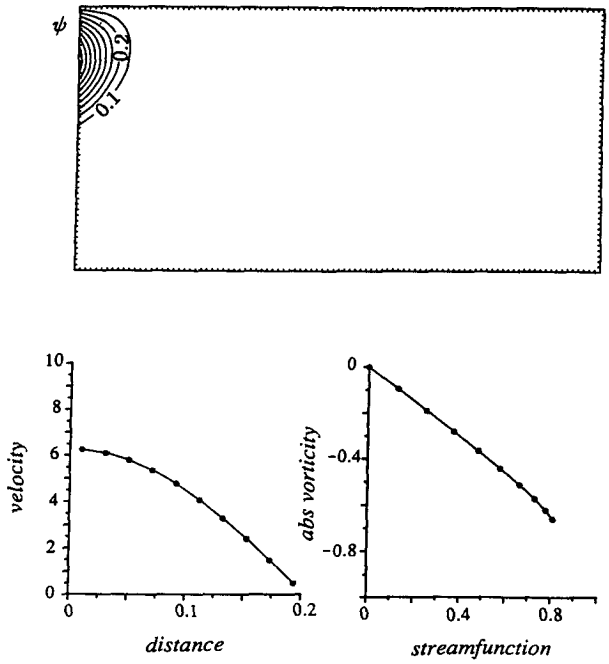

FIG. 8. The steady-state solution obtained when a sine jet is prescribed. Now the absolute vorticity is a nonlinear function of the streamfunction, across the inflow, but the underlying α is negative; a modon-type recirculation is obtained.

study focuses exclusively on inertial control in a regime where frictional effects are unimportant and penetration is controlled by the cross-stream velocity profile. To verify that our results are, to first approximation, independent of the level of biharmonic friction, we have performed a series of experiments in which the frictional coefficient takes on a range of values. The inflow from the experiment in section 3b(6) is used, in which $\chi = 0.3$. In Fig. 11, jet penetration, measured by the most easterly point reached by the $\psi = 0.1$ contour, is plotted as a function of the magnitude of the biharmonic friction coefficient (normalized with respect to our reference value $\beta\Delta^5$). Jet penetration is, to a first approximation, independent of frictional coefficient until a value one order of magnitude larger than that used in our experiments is reached. Reducing ν by an order of magnitude leads to no change in penetration scale, but the vorticity field is somewhat noisier on the scale of the grid.

4. The penetration of a jet in a stratified ocean

Here we consider injecting a fluid into a basin from an inertial jet that has both vertical and horizontal structure. The degree to which the jet penetrates is controlled by the extent to which the inflow projects onto either the baroclinic Fofonoff gyres of Marshall and Nurser (1986) or a baroclinic generalization of the modon. First, the relevant theory is introduced, followed by supporting numerical experiments with a 2- and 3-layer version of our quasigeostrophic ocean model. In an analogous way to the barotropic model, the key parameter in our baroclinic model is $\alpha_A = dq_A/d\Psi_A$, but where q_A and Ψ_A are now the absolute vorticity and streamfunction associated with the *pseudo* barotropic mode.

a. The 2-layer model

For convenience, we carry out our analysis in a model having two layers of equal depth with a density jump in between. This 2-layer model provides an illuminating insight into the penetration properties of a baroclinic jet. The quasigeostrophic potential vorticity of the two moving layers is defined thus:

$$Q_1 = \nabla^2\psi_1 + \beta y - F(\psi_1 - \psi_2), \qquad (23a)$$

$$Q_2 = \nabla^2\psi_2 + \beta y - F(\psi_2 - \psi_1). \qquad (23b)$$

In the upper layer, for analytical convenience, we assume a linear functional relationship between the streamfunction and the potential vorticity. In the second layer it is assumed, following Rhines and Young (1982) and as in Marshall and Nurser (1986, 1988), that eddies homogenize the potential vorticity to the value of the planetary vorticity on the northern boundary of the gyre:

$$Q_1 = \gamma\psi_1 - c, \qquad (24a)$$

$$Q_2 = 0. \qquad (24b)$$

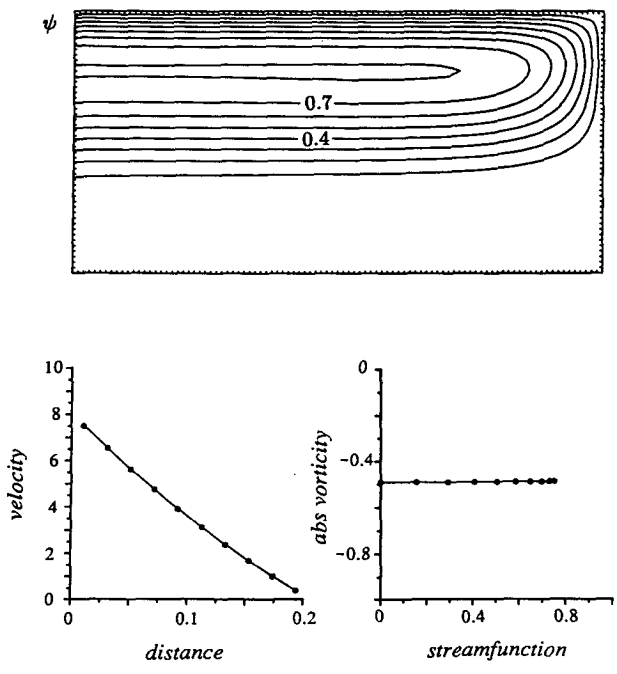

FIG. 9. The steady-state response to a uniform absolute vorticity jet inflow. The resulting circulation is Fofonoff-like.

Two linearly-independent modes can be identified, which will be called "pseudomodes,"[1] defined by

$$\Psi_A = \cos\eta_A\psi_1 + \sin\eta_A\psi_2, \tag{25a}$$

$$\Psi_B = \cos\eta_B\psi_1 + \sin\eta_B\psi_2, \tag{25b}$$

where

$$\tan\eta_{A,B} = \lambda \pm \sqrt{1+\lambda^2}, \tag{26}$$

$$\lambda = \gamma/2F. \tag{27}$$

As shown in appendix B, Eqs. (25a) and (25b) can be neatly inverted to find the projections of the pseudomodes onto each layer, thus:

$$\psi_1 = -\sin\eta_B\Psi_A + \sin\eta_A\Psi_B, \tag{28a}$$

$$\psi_2 = \cos\eta_B\Psi_A - \cos\eta_A\Psi_B. \tag{28b}$$

The absolute vorticities for the pseudomodes,

$$q_{A,B} = \nabla^2\Psi_{A,B} + \beta_{A,B}y, \tag{29}$$

are linearly related to the corresponding streamfunctions, that is,

$$q_{A,B} = \alpha_{A,B}\Psi_{A,B} - c_{A,B}, \tag{30}$$

where $\alpha_{A,B}$ is given by

$$\alpha_{A,B} = \frac{\gamma + 2F}{2} \mp F\sqrt{1+\lambda^2}. \tag{31}$$

The effective planetary vorticity gradients felt by each mode are

$$\beta_{A,B} = \beta\cos\eta_{A,B}(1 + \tan\eta_{A,B}), \tag{32}$$

and

$$c_{A,B} = c\cos\eta_{A,B}. \tag{33}$$

Now we show that the important quantity controlling penetration is α_A, the eigenvalue of the "pseudobarotropic" mode analogous to the α of our 1½-layer model. On examining Eq. (31) and using Eq. (27), it is seen that $\alpha_A = 0$ when $\gamma = 0$. We now examine the two cases in which $\alpha_A > 0$ ($\gamma > 0$) and $\alpha_A < 0$ ($\gamma < 0$).

1) PENETRATING JETS: $\alpha_A > 0$

This class of jets is similar to the boundary currents of the baroclinic Fofonoff gyres of Marshall and Nurser (1986, 1988). Both α_A and α_B are positive, and the discussion of section 2b can be extended to show that c must be positive if we are to have an anticyclonic gyre. The structure of our inflowing jet can be readily written down by making use of our modes.

[1] Note that when $\gamma = 0$, our modes reduce to the usual barotropic and baroclinic modes.

The first mode has the form of a Fofonoff-gyre solution,

$$\Psi_A = \frac{c_A}{\alpha_A}\left\{\frac{\beta_A y}{c_A} + 1 - e^{\sqrt{\alpha_A}y}\right\}, \tag{34}$$

as does the second mode,

$$\Psi_B = \frac{c_B}{\alpha_B}\left\{\frac{\beta_B y}{c_B} + 1 - e^{\sqrt{\alpha_B}y}\right\}. \tag{35}$$

These modes must now be projected onto each layer using Eqs. (28a) and (28b). The projection of Ψ_A onto each layer is positive, but the projection of Ψ_B is of a different sign in each layer: positive (negative) onto the top (lower) layer. There are two regions of interest. In the upper layer of the eastward-flowing northern boundary current, the pseudobaroclinic mode reinforces the negative relative vorticity from the pseudobarotropic mode, while in the lower layer, it tends to cancel the pseudobarotropic relative vorticity in a manner required to ensure that Q_2 is homogenized. Penetration occurs in both layers of the solution. However, in the returning zonal flow to the south, the second mode increases the current in the lower layer while reducing the current in the upper layer. This has the effect of moving the bounding streamline in layer 2 north from that predicted by the pseudobarotropic mode alone (with the opposite effect in the upper layer). South of the bounding streamline, the lower layer is at rest, and the remaining recirculating water returns in the upper layer in a manner described by the "stacked" Fofonoff gyres of Marshall and Nurser (1986).

Choosing a value of $\gamma = F/2$ implies a positive eigenvalue for the pseudobarotropic mode; Eq. (31) gives $\alpha_A = 0.22F$ and $\alpha_B = 2.28F$. The pseudomodes are given by Eqs. (34) and (35), and, projecting back onto the layers, the following expressions for ψ_1 and ψ_2 are obtained:

$$\psi_1 = \frac{\beta y_0}{F}\left\{4.0\frac{y}{y_0} + 2.0 - 1.72e^{\sqrt{0.22F}y} - 0.28e^{\sqrt{2.28F}y}\right\}, \tag{36a}$$

$$\psi_2 = \frac{\beta y_0}{F}\left\{5.0\frac{y}{y_0} + 2.0 - 2.21e^{\sqrt{0.38F}y} + 0.21e^{\sqrt{2.28F}y}\right\}. \tag{36b}$$

These solutions were used to prescribe the inflow to our numerical model, now extended to allow two moving layers above a flat bottom, but otherwise as described before. We choose a value of $F = (0.05L)^{-2}$ corresponding to a Rossby radius of 25 km for L = 500 km. The results are displayed in Fig. 12, together with plots of the inflow jet profiles. Penetration readily occurs, and the recirculation closely resembles the form predicted by the analytical solution. Note in particular the difference between the meridional scales in layers

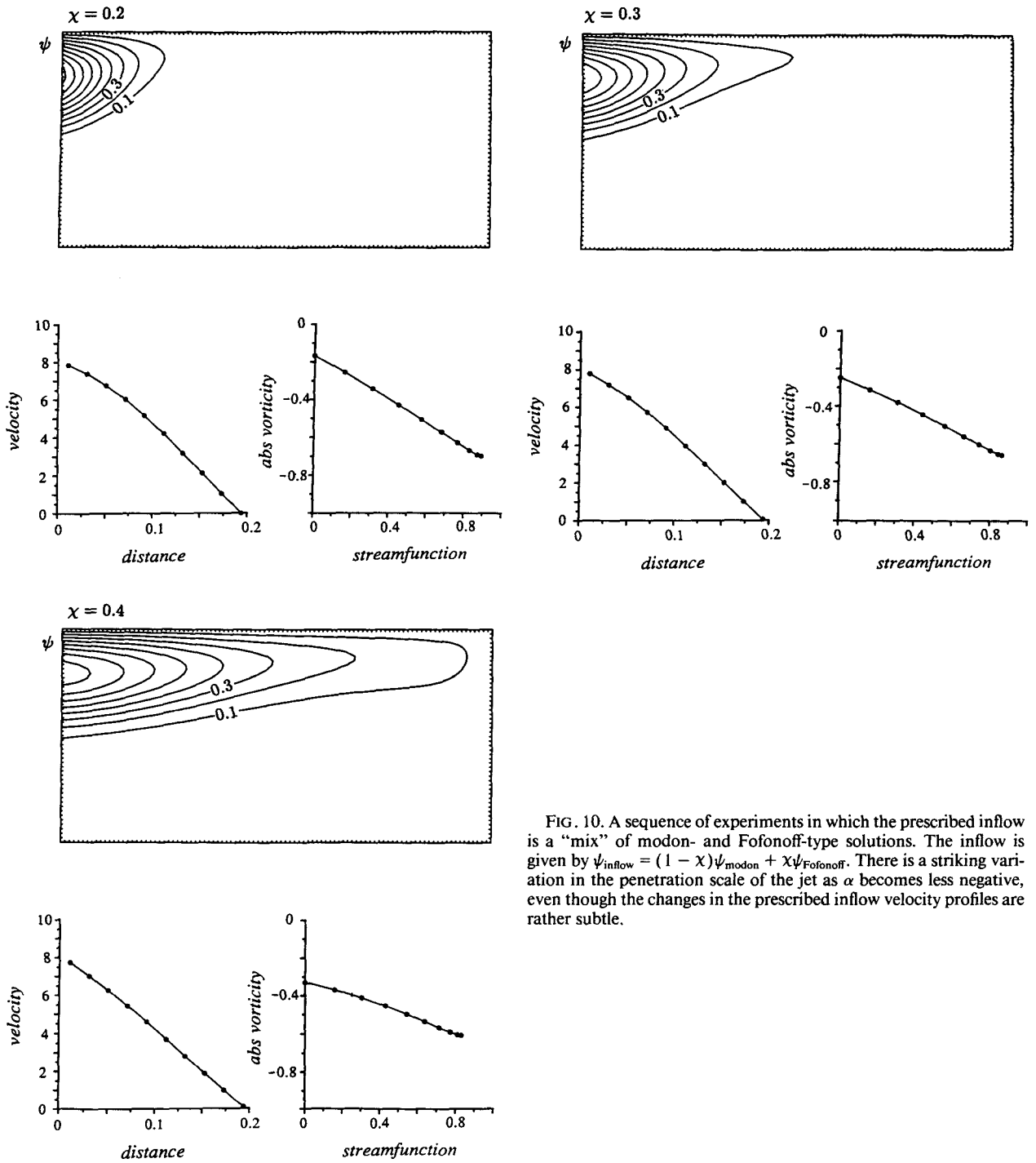

FIG. 10. A sequence of experiments in which the prescribed inflow is a "mix" of modon- and Fofonoff-type solutions. The inflow is given by $\psi_{\text{inflow}} = (1 - \chi)\psi_{\text{modon}} + \chi\psi_{\text{Fofonoff}}$. There is a striking variation in the penetration scale of the jet as α becomes less negative, even though the changes in the prescribed inflow velocity profiles are rather subtle.

1 and 2, as predicted by the analysis in the preceding sections, and a characteristic feature of the baroclinic Fofonoff gyres of Marshall and Nurser (1986).

2) RECIRCULATING JETS: $\alpha_A < 0$

These jets are characterized by a negative value of α_A. For analytical convenience, we will consider the case in which $c = 0$. A modon solution for the pseudobarotropic mode satisfying Eqs. (29) and (30) can be written as

$$\Psi_A = \left\{ AJ_1(kr) - \frac{\beta_A r}{k^2} \right\} \sin\theta, \tag{37}$$

where $k^2 = -\alpha_A$, and A is a constant.

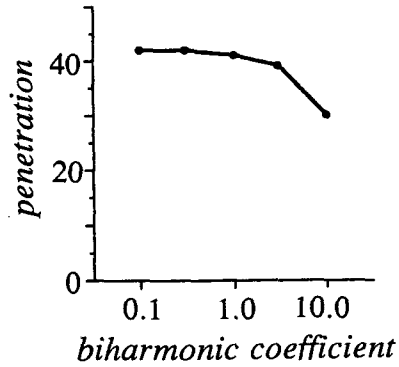

FIG. 11. The sensitivity of jet penetration to the level of biharmonic friction. Details of the inflow can be found in the text. The penetration, defined as the most easterly point reached by the $\psi = 0.1$ contour, is plotted in units of grid size (the eastern boundary is at 96). The biharmonic diffusion coefficient is normalized with respect to our reference value $\beta\Delta^5$.

For the pseudobaroclinic mode, it can be shown that α_B is always positive, so a modon-type solution is not appropriate. However, a particular integral corresponding to a zonal flow is

$$\Psi_B = -\frac{|\beta_B| r}{\alpha_B} \sin\theta, \qquad (38)$$

where for clarity, the modulus of β_B is taken since β_B is always negative when α_A is negative. Equation (38) satisfies only the boundary condition on the northern wall. However, anticipating recirculating behavior, we are not concerned with the need to satisfy an eastern boundary condition.

When the above two modes [Eqs. (37) and (38)] are projected onto each layer, two different modon solutions with modified radii and amplitudes are obtained. At first sight, this is a surprising result, but it arises because a modon solution consists of the sum of two elements: a bessel-function perturbation and a zonal flow. By adding or subtracting an additional zonal flow we merely alter the relative magnitude of these two terms, thus changing the amplitude and radius of our solution. The effect of projecting the two modes onto the second layer is to create a modon of reduced radius. In a similar way, the recirculation radius in layer 1 will be increased.

Choosing a value of $\gamma = -1.5F$ gives $\alpha_A = -F$, $\alpha_B = 1.5F$. The solutions for the two layers, constructed from the two pseudomodes, are then

$$\psi_1 = \beta F^{-3/2}\{-13.4 J_1(\sqrt{Fr}) - 1.0\sqrt{Fr}\} \sin\theta, \qquad (39a)$$

$$\psi_2 = \beta F^{-3/2}\{-6.7 J_1(\sqrt{Fr}) - 1.0\sqrt{Fr}\} \sin\theta, \qquad (39b)$$

where in Eq. (37) A has been given the value $-15\beta_A F^{-1.5}$ to give a realistic jet magnitude.

A numerical experiment was performed with the above inflow profile. Here F was chosen to have a value $(0.1L)^{-2}$, implying a Rossby radius of 50 km if L = 500 km. The steady-state solution from the numerical model, together with the inflow profile, are shown in Fig. 13. In both layers the gyre recirculates tightly, in a nonpenetrative manner, and the recirculation extends farther in the upper layer than in the lower layer, entirely in accord with the above analysis.

Hence, it is seen that α_A, the eigenvalue associated with the pseudobarotropic mode, determines the penetration properties of our baroclinic jet. When α_A is positive, the baroclinic jet penetrates across to the eastern boundary of the basin; when α_A is sufficiently negative, the jet recirculates tightly. In both cases, α_B is positive, but the pseudobaroclinic mode merely introduces baroclinic structure into the jet; it does not control its penetrative behavior.

b. *The continuously stratified model*

We began our discussion by stating that α_A would be instrumental in determining the penetration character of our jet and have shown this to be the case in

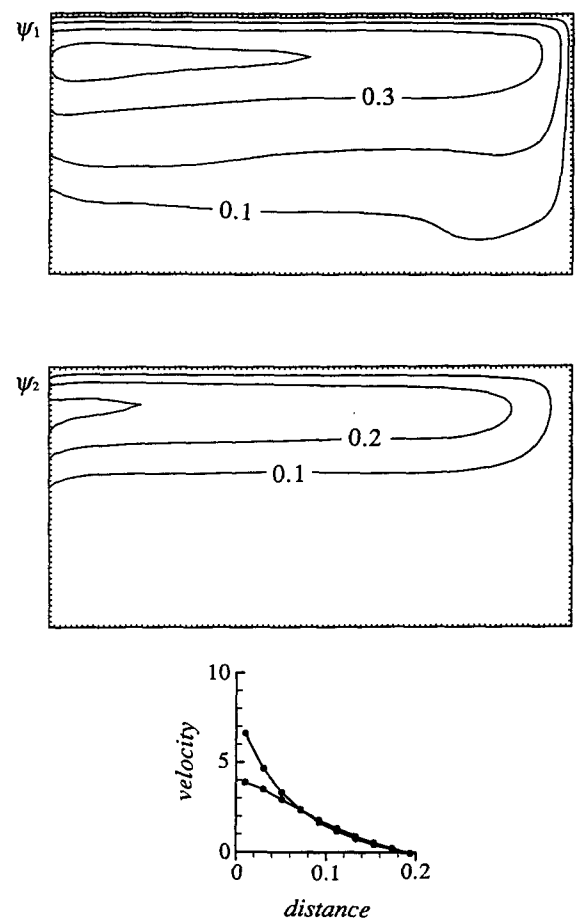

FIG. 12. The steady state resulting from a prescribed baroclinic Fofonoff-type inflow in a 2-layer model in which $\alpha_A = 0.22F$. The meridional scales of the return flow are in broad agreement with the analytical solution.

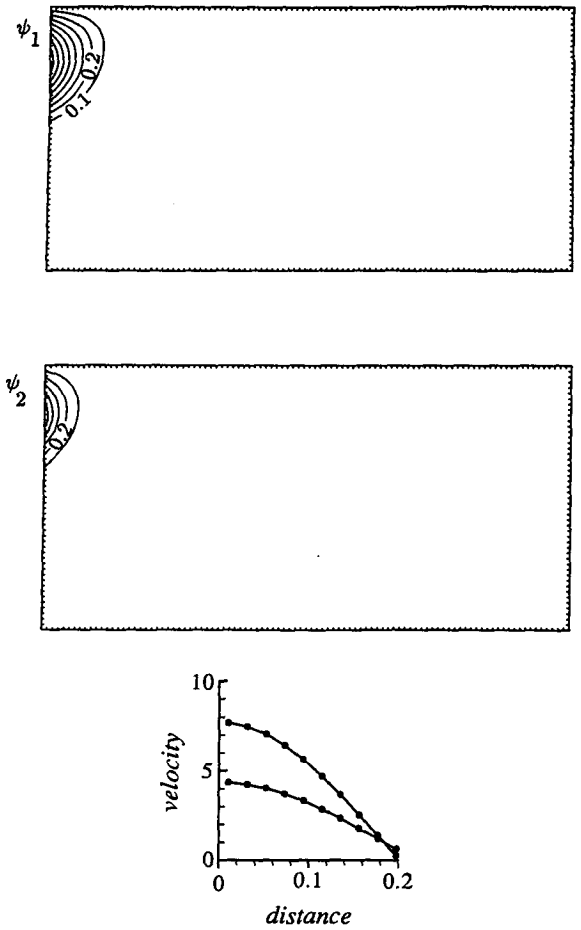

FIG. 13. The steady state resulting from a prescribed baroclinic modon-type inflow in a 2-layer model in which $\alpha_A = -1.0F$. Note the different recirculation scales in each layer, diminishing with depth, as suggested by our analysis.

a 2-layer system. The above ideas are easily extended to many layers, although the analysis quickly becomes rather tedious. Two experiments have been performed with a 3-layer model, with equal layer depths and equal density jumps between them, to illustrate how our ideas carry over to models with a more realistic vertical structure. In the first, the eigenvalue, α_A, of the pseudobarotropic mode takes on a positive value with

$$\alpha_A = 0.06F, \quad \alpha_B = 1.1F, \quad \alpha_C = 3.0F,$$

and $F = (0.05L)^{-2}$ implying Rossby radii of 25 km and 14.4 km if $L = 500$ km. In the second experiment, α_A is negative with

$$\alpha_A = -1.0F, \quad \alpha_B = 0.6F, \quad \alpha_C = 2.8F,$$

and $F = (0.1L)^{-2}$ implying Rossby radii of 50 km and 28.8 km if $L = 500$ km.

In calculating the jet inflow profiles, we assumed that the potential vorticity is homogeneous in the two subsurface layers. The steady states from the numerical experiments are plotted in Figs. 14 and 15. As expected, in the first experiment where $\alpha_A > 0$, the jet penetrates across to the eastern boundary in each layer. In the second experiment, $\alpha_A < 0$ and the jet recirculates tightly in roughly circular regions that diminish in radius with depth. This is entirely in accord with our foregoing analysis.

In the continuously stratified model, as noted by Greatbatch (1988), there are an infinite set of pseudomodes, Ψ_A, Ψ_B, Ψ_C, . . . , and a corresponding set of eigenvalues, $\alpha_A < \alpha_B < \alpha_C <, \ldots$. A finite number of these eigenvalues may be negative, and the most

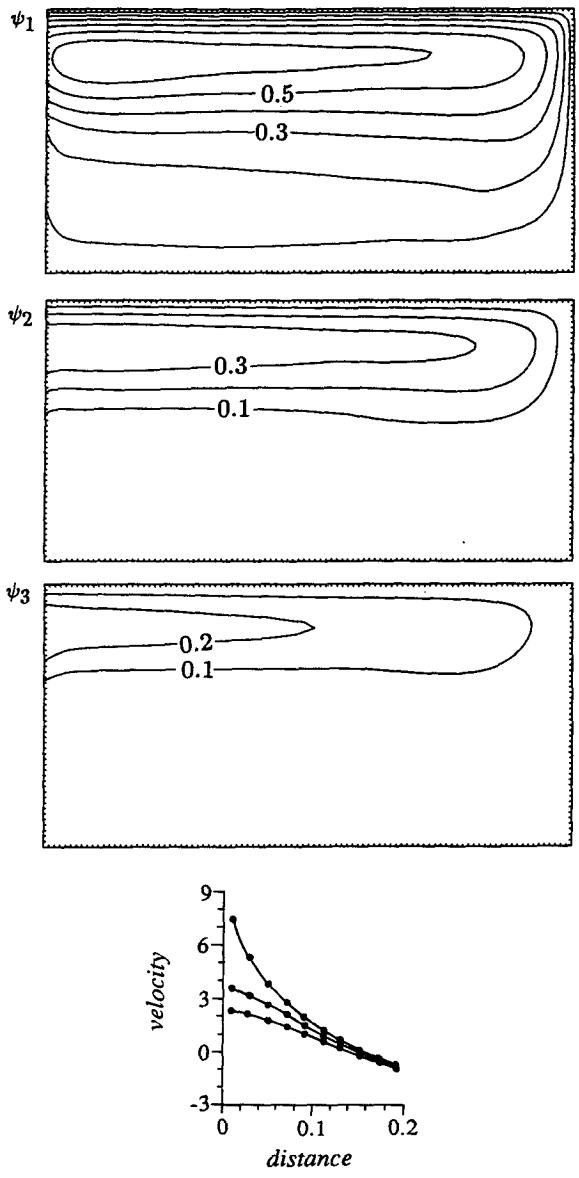

FIG. 14. The steady state resulting from a 3-layer baroclinic inflow in which $\alpha_A = 0.06F$. Note that the flow in the upper layer is cusplike as sketched schematically in Fig. 1a. The jet penetrates across to the eastern boundary in all three layers.

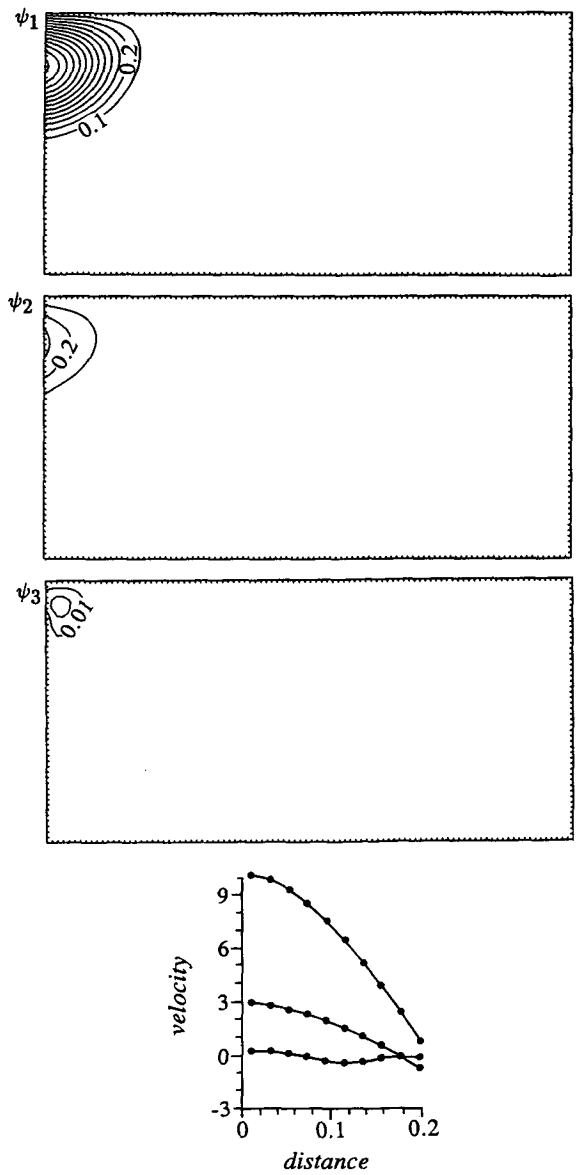

FIG. 15. The steady state resulting from a 3-layer baroclinic inflow in which $\alpha_4 = -1.0F$. Note the flow in layer 1 is wave-like as sketched schematically in Fig. 1b. The recirculation is tight in all three layers. Note that the contour interval is a factor of 10 smaller in layer 3 where the flow is extremely weak.

negative eigenvalue will belong to the pseudobarotropic mode. In the case that all the eigenvalues are positive, our jets will be described by the continuously stratified baroclinic Fofonoff gyres of Greatbatch (1987), and we expect penetration. Conversely, if the pseudobarotropic mode is sufficiently negative, we anticipate that recirculation will occur. In analogy with the 2-layer and 3-layer systems, we predict that the first mode will determine the underlying behavior of the jet and that additional modes will serve only to modify the baroclinic structure. This idea is reinforced by the observation that downstream velocity profiles of the Gulf Stream are likely to strongly project onto the pseudobarotropic mode; there is little evidence of major reversals of current with depth, and it is observed to be surface intensified. The pseudobarotropic mode is also strongly surface intensified (because $dQ/d\psi$ is so negative near the surface), and there are no nodes in the vertical.

5. Jet penetration in numerical models

In the foregoing experiments we have shown that subtle changes in the cross-stream velocity profile of a seaward-flowing inertial jet can have a marked effect on its penetration properties. This suggests that jet dynamics will be highly sensitive to the formulation of a numerical model and its resolution. We briefly mention three important modeling issues here that our study may illuminate.

a. The barotropic model

Equation (4) admits an infinite number of solutions in the absence of forcing and dissipation; in purely free inviscid flow α can be ascribed any value. However, in the presence of weak forcing and dissipation, α cannot be freely chosen. For example, a plausible balance over closed streamlines between wind stress curl forcing and downgradient fluxing of potential vorticity by the geostrophic eddy field requires that

$$\frac{dQ}{d\psi} < 0 \tag{40}$$

(Niiler 1966; Rhines and Young 1982; Marshall and Nurser 1986). In a barotropic model, this immediately implies that α is negative, hence excluding the possibility of a penetrating jet. Indeed, barotropic models of ocean circulation are characterized by recirculating, rather than penetrating, jets (for example, see Böning 1986). However, in a 1½-layer model, or an N-layer model, the stretching term in the potential vorticity enables α to be greater or less than zero, permitting both penetration and recirculation while satisfying Eq. (40) in near-surface layers.

b. Horizontal resolution of a numerical model

Solutions for a subtropical gyre, in which α is positive, necessarily have low values of absolute vorticity on the northern boundary. Conversely, solutions for a subpolar gyre, in which α is positive, have high values of absolute vorticity on the southern boundary. What happens, then, in a double-gyre configuration? Given a model with infinite resolution, a discontinuity in the absolute vorticity field at the confluence of the gyres would be represented. However, at finite resolution, as is the case in a numerical model, the q profile as seen by the model, q^* (Fig. 16), may be very different; a

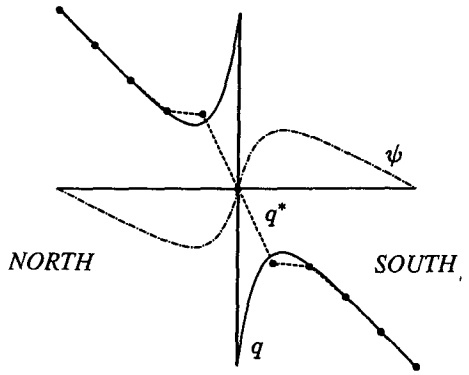

FIG. 16. A schematic diagram demonstrating how finite-grid resolution may change the sign of $dq/d\psi$ as "seen" by a numerical model. Here ψ and q are the analytical forms for the streamfunction and the absolute vorticity; q^* is the absolute vorticity as obtained by a crude finite difference calculation (the markers indicate the location of grid points). If the grid resolution is much smaller than the width of the jet, the volume of fluid in which α changes sign will be negligible. However, at coarse resolution, this volume will be large, dramatically changing the subsequent behavior of the jet.

small region will exist in which α changes sign. This is illustrated in Fig. 16 where, at very coarse resolution, the model may well interpret the jet as a region in which α is negative.

Experiments have been performed to investigate whether change in penetration properties results from poor model resolution. In order to represent the double gyre, a symmetry condition was adopted along the northern wall of our subtropical gyre:

$$(\nabla^2\psi)_{y=0} = 0. \qquad (41)$$

Figure 17 shows the results of identical runs with a Fofonoff-type jet inflow imposed as in section 3b(1), but at two model resolutions: one with 49 grid points in the north–south direction (10-km resolution) and the other with a resolution of 21 grid points (25-km resolution). The former yields a Fofonoff-type solution, while in the latter case, the jet recirculates in the manner of modon, a consequence of poor model resolution; the cusplike jet profile cannot be represented in the low-resolution model and is seen as a wavelike profile.

Barnier et al. (1991) present a detailed study of the effect of changing horizontal and vertical resolution on an eddy-resolving double-gyre experiment. They conclude that the most striking change on increasing the horizontal resolution is, indeed, to facilitate the resonance of inertial modes and increase jet penetration. It seems that at 10-km resolution they can resonantly excite Fofonoff's (1954) mode, leading to penetrating rather than recirculating behavior.

c. *Lateral boundary conditions*

The role of boundary conditions along the western margin of ocean basins, and their possible impact on the penetration of emergent jets, have been discussed before (Marshall 1982). There it was argued that a no-slip boundary condition along the western boundary reduces the penetration of a jet as compared to a free-

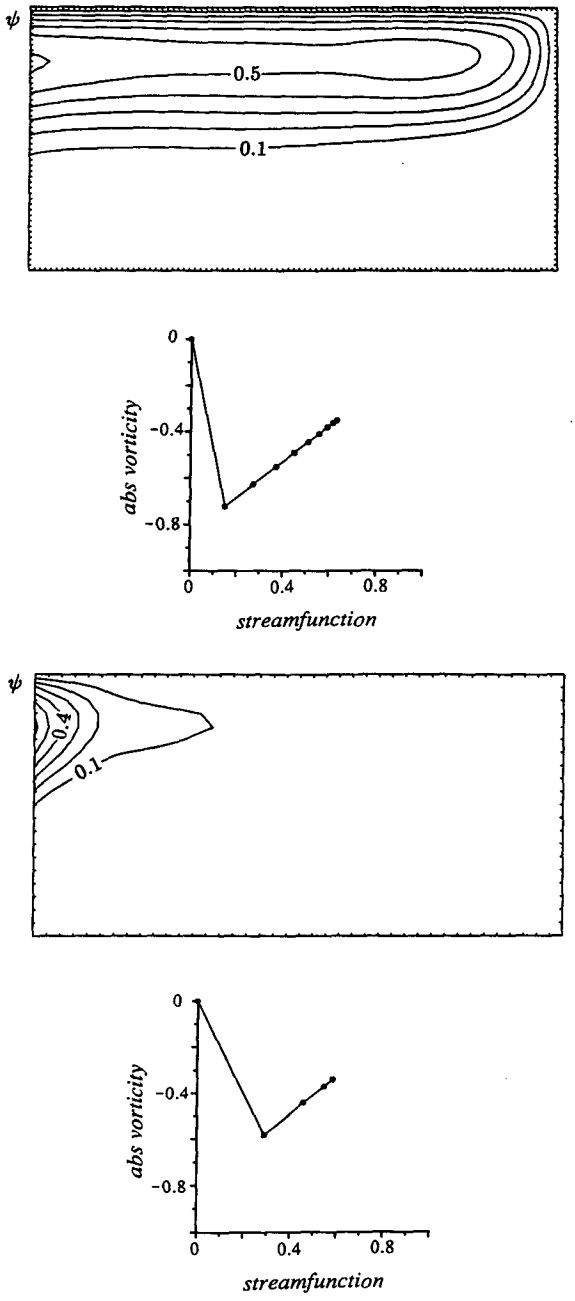

FIG. 17. Results of two identical experiments in which a Fofonoff-type inflow has been prescribed. In the first experiment, a resolution of 97 × 49 grid points (corresponding to ten across the jet) has been used; in the second, a resolution of 41 × 21 grid points (only four across the jet) has been employed. There is a dramatic change in penetration properties. Notice how α reverses sign near the northern boundary; in the poorly resolved run, this region completely dominates the dynamics of the jet.

slip condition. This is readily understood in the context of our present work.

Imagine, as illustrated schematically (Fig. 18), fluid parcels moving from the Sverdrup interior being swept northward into a western boundary current. If free-slip conditions are assumed, fluid parcels near the boundary will conserve potential vorticity, resulting in anomalously low values of relative vorticity in the northwestern corner of the subtropical gyre. On separation from the wall, these fluid parcels form an intense jet with $\alpha > 0$ and Fofonoff behavior. However, if a no-slip boundary condition is assumed, a viscous sublayer results in which relative vorticity diffuses in from the boundary. The absolute vorticity of the water closest to the western boundary must be positive to satisfy the no-slip condition. On emerging to form a seaward jet, water that has passed through the sublayer will have a negative α; if the sublayer is wide, it will dominate the behavior of the jet, leading to recirculation rather than penetration. Indeed, barotropic models of the subtropical gyre in which no-slip conditions are applied are characterized by tight recirculating gyres in the northwestern corner of the basin. In complete contrast, penetrating inertial gyres are obtained in the limit of weak dissipation when no-slip boundary conditions are assumed (e.g., Pedlosky 1979). Which, no-slip or free-slip, is the appropriate condition to assume in a large-scale model is still unknown.

6. Concluding remarks

It has been shown that the distribution of absolute vorticity across a jet can strongly influence its zonal scale of penetration by exciting one or the other of two classes of free-mode solutions depending upon the sign of $\alpha = dq/d\psi$. Whether the jet penetrates or recirculates depends on the degree to which it "projects" onto the classes of "free-mode" solutions, prototypical examples of which are the Fofonoff gyre ($\alpha > 0$) and the modon ($\alpha < 0$). In a jet with both vertical and horizontal structure, it is the α associated with the "pseudobarotropic" mode that controls the penetrative behavior. We have seen that subtle changes to the velocity structure of a jet can have marked effects on its behavior. A corollary of our study is the importance it attaches to resolving adequately both the vertical and horizontal structure of intense jets, such as the Gulf Stream, in models of gyres. It may provide, in part, an interpretation of some of the results of Barnier et al. (1991). They, however, propose a subtle role for the higher baroclinic modes in controlling the energy cascade of an unstable jet. Instead, here we emphasize the importance of the gravest (pseudobarotropic) vertical mode in controlling the free, inertial behavior of a jet.

The study also provides a context for the study of Cessi et al. (1987) and Ierley and Young (1988). In the two aforementioned papers, uniform absolute vorticity solutions are investigated (i.e., $\alpha = 0$), and so, as we have seen, inertial effects do not constrain the east–west scale. In this case, eddy processes must come into play in setting the penetration. However, in the more general case where α is nonzero, the inertial effects considered here may play a dominant role.

Acknowledgments. We wish to thank Roger Brugge for his assistance with the numerical aspects of this work and the anonymous reviewers for their helpful comments. David Marshall is supported by the Natural Environment Research Council, United Kingdom, and in part by NSF 9115915-OCE.

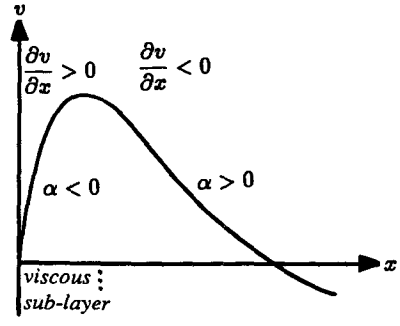

FIG. 18. A schematic diagram illustrating the implication of a no-slip boundary condition on the absolute vorticity profile across a jet. Since the tangential velocity on the wall vanishes, $\partial v/\partial x > 0$ at the boundary, and so in the viscous sublayer, strong cyclonic vorticity is present in the flank of the northward-flowing current. If the viscous layer is of a comparable width to the boundary current, then the "effective" α will be negative, resulting in recirculating rather than penetrating behavior.

APPENDIX A

Radiation Boundary Conditions

Radiation boundary conditions prescribe the time evolution of the streamfunction field on the open western boundary of our model, according to a recipe by Miller and Thorpe (1981). The equation on which this is based is

$$\frac{\partial \phi}{\partial t} = c\frac{\partial \phi}{\partial x}, \tag{A1}$$

where c is a velocity that includes both wave propagation and advection and ϕ is the property of the fluid that is to be radiated across the boundary. In our particular application, ϕ is the velocity component normal to the boundary.

The velocity c is calculated from adjacent grid points at the two previous time steps:

$$c = \frac{\partial \phi/\partial t}{\partial \phi/\partial x} = \frac{\Delta}{\Delta t}\left(\frac{\phi_2^{n-1} - \phi_2^{n-2}}{\phi_1^{n-2} - \phi_2^{n-2}}\right), \tag{A2}$$

where the superscript refers to the time level, and the subscript labels the grid point.

Here Δt is the time-step interval and Δ is the grid spacing. Combining (A1) and (A2) gives the numerical recipe

$$\phi_1^n = \phi_1^{n-1} + (\phi_1^{n-1} - \phi_2^{n-1})\left(\frac{\phi_2^{n-1} - \phi_2^{n-2}}{\phi_1^{n-2} - \phi_2^{n-2}}\right). \quad \text{(A3)}$$

If $\phi_2^{n-1} = \phi_1^{n-1}$, then ϕ_1^n is set to ϕ_1^{n-1}. If c is positive, corresponding to an inflow, then ϕ_1^n is given by ϕ_1^{n-1}; if c is greater than $(\Delta/\Delta t)$, then ϕ_1^n is set equal to ϕ_2^{n-1}.

The streamfunction values bounding the radiative region are required to remain constant in time. Any discrepancy between these values and values implied by the radiative scheme are removed by adding or subtracting an appropriately weighted amount from each radiatively calculated normal velocity component.

APPENDIX B

Derivation of Projection of Pseudomodes onto Layers

Here we detail the derivation of Eqs. (28a) and (28b). The pseudomodes are defined by Eqs. (25a) and (25b). Multiplying Ψ_A by $\cos\eta_B$, and Ψ_B by $\cos\eta_A$, and taking the difference, we obtain

$$\sin(\eta_A - \eta_B)\psi_1 = -\sin\eta_B\Psi_A + \sin\eta_A\Psi_B. \quad \text{(A4a)}$$

Similarly,

$$\sin(\eta_A - \eta_B)\psi_2 = \cos\eta_B\Psi_A - \cos\eta_A\Psi_B. \quad \text{(A4b)}$$

Using the identity,

$$\sin(\eta_A - \eta_B) = \cos\eta_A\cos\eta_B(\tan\eta_A - \tan\eta_B),$$

and substituting for $\tan\eta_{A,B}$ from Eq. (26), we obtain

$$\sin(\eta_A - \eta_B) = 2\sqrt{1 + \lambda^2}\cos\eta_A\cos\eta_B$$

But, making use of the trigonometric identity

$$\cos x = \frac{1}{\sqrt{1 + \tan^2 x}},$$

together with Eq. (26), it follows that

$$\cos\eta_A\cos\eta_B = \frac{1}{2\sqrt{1 + \lambda^2}}.$$

Thus,

$$\sin(\eta_A - \eta_B) = 1, \quad \text{(A5)}$$

and so Eqs. (A4a) and (A4b) reduce to the expressions for ψ_1 and ψ_2 quoted in Eqs. (28a) and (28b).

REFERENCES

Barnier, B., B. L. Hua, and C. Le Provost, 1991: On the catalytic role of high baroclinic modes in eddy-driven large-scale circulations. *J. Phys. Oceanogr.*, **21**, 976–997.

Böning, C., 1986: On the influence of frictional parameterization in wind driven ocean circulation models. *Dyn. Atmos. Oceans.*, **10**, 63–92.

Cessi, P., G. Ierley, and W. Young, 1987: A model of the inertial recirculation driven by potential vorticity anomalies. *J. Phys. Oceanogr.*, **17**, 1640–1652.

Fofonoff, N. P., 1954: Steady flow in a frictionless homogeneous ocean. *J. Mar. Res.*, **13**, 254–262.

——, 1962: Dynamics of ocean currents. *The Sea, Vol. 1: Physical Oceanography*, M. N. Hill, Ed., Wiley-Interscience.

Greatbatch, R. J., 1987: A model for the inertial recirculation of a gyre. *J. Mar. Res.*, **45**, 601–634.

——, 1988: On the scaling of inertial subgyres. *Dyn. Atmos. Oceans*, **12**, 265–285.

Holland, W. R., and W. J. Schmitz, 1985: Zonal penetration scale of model midlatitude jets. *J. Phys. Oceanogr.*, **15**, 1859–1875.

Ierley, G., and W. Young, 1988: Inertial recirculation in a β-plane corner. *J. Phys. Oceanogr.*, **18**, 683–689.

Larichev, V. D., and G. M. Reznik, 1976: Two-dimensional Rossby soliton: An exact solution. *POLYMODE News*, No. 19, 3 and 6.

Marshall, J. C., 1982: The vorticity equilibrium of ocean gyres and vorticity boundary conditions. *Ocean Modelling*, **47**, 1–3.

——, and G. Nurser, 1986: Steady, free circulation in a stratified quasigeostrophic ocean. *J. Phys. Oceanogr.*, **16**, 1799–1813.

——, and ——, 1988: On the recirculation of the subtropical gyre. *Quart. J. Roy. Meteor. Soc.*, **114**, 1517–1534.

——, ——, and R. Brugge, 1988: On the time-averaged flow of quasigeostrophic wind-driven gyres. *J. Geophys. Res.*, **93**, 15 427–15 436.

Miller, M. J., and A. J. Thorpe, 1981: Radiation conditions for the lateral boundaries of limited-area numerical models. *Quart. J. Roy. Meteor. Soc.*, **107**, 615–628.

Niiler, P. P., 1966: On the theory of wind-driven ocean circulation. *Deep-Sea Res.*, **13**, 597–606.

Pedlosky, J., 1979: *Geophysical Fluid Dynamics*. Springer-Verlag, 710 pp.

Rhines, P. B., and W. R. Young, 1982: A theory of wind-driven circulation, I. Mid-ocean gyres. *J. Mar. Res.*, **40** (Suppl), 559–596.

Stern, M. E., 1975: Minimal properties of planetary eddies. *J. Mar. Res.*, **33**, 1–13.